Regular Paper

Journal of Electroanalytical Chemistry

Electrochemical and spectroelectrochemical probing of the ionic channel in Nafion films using the redox of perfluoroalkyl viologen

Tatsuya Ayabe[a], Aicheng Chen[b], Takamasa Sagara[c*]

[a]*Department of Advanced Technology and Science for Sustainable Development, Graduate School of Engineering, Nagasaki University, Bunkyo 1-14, Nagasaki 852-8521, Japan*

[b]*Electrochemical Technology Centre, Department of Chemistry, University of Guelph, 50 Stone Rd E., Guelph, Ontario N1F 2W1, Canada*

[c]*Division of Chemistry and Materials Science, Graduate School of Engineering, Nagasaki University, Bunkyo 1-14, Nagasaki 852-8521, Japan*

Keywords:

Nafion film

Ionic channel

Chemical micro-environment

Perfluoroalkyl viologen

Electroreflectance

*Corresponding author.

E-mail address: sagara@nagasaki-u.ac.jp

ABSTRACT

We explored the electrochemistry of a perfluoroalkyl viologen, *N*,*N*'-di-(1*H*,1*H*,2*H*,2*H*-perfluorobutyl)-4,4'-bipyridinium dichloride (FC4VFC4) in a Nafion film on an Au electrode. The capability of FC4VFC4 as a redox-active probe for micro-environments of the ionic channels in the Nafion film was highlighted by clarifying the difference of its electrochemical behavior from that of its alkyl analog, dibutyl viologen (C4VC4). The time course of cyclic voltammograms (CVs) was tracked after immersion of a Nafion film-coated Au electrode in viologen solutions of various concentrations, C_s. The strongly C_s-dependent time change revealed the formation of an aggregate of FC4VFC4 in the ionic channels in the Nafion film. The aggregate blocks its own redox reaction at $C_s \geq 10$ μM. At $C_s = 5$ μM, FC4VFC4 exhibited a quasi-reversible response. In contrast, C4VC4 showed a quasi-reversible response in the C_s range from 5 μM to 200 μM. We also used the time dependent change of electroreflectance (ER) spectra to track the state of viologens in the close proximity of the electrode|Nafion interface. After the immersion in 50 μM FC4VFC4 solution, the ER signals of the redox of FC4VFC4 molecules, being not in direct contact with the Au surface, rapidly increased in line with the change of CVs. What followed was a steep decrease of ER signal while the CV redox current was still increasing. It was also found that the FC4VFC4 aggregates in the Nafion film block the electrode reactions of $[Ru(NH_3)_6]^{2+/3+}$, methylviologen, and C4VC4, which otherwise show reversible or quasi-reversible responses in the absence of FC4VFC4. All the results, especially the sharp contrast of the behavior of FC4VFC4 to that of C4VC4, revealed that either or both intermolecular perfluoro chain-chain interaction and perfuorinated FC4VFC4 side chain-Nafion perfluoroether side chain interaction are the key to determine the chemical micro-environment in the ionic channels.

1. Introduction

Proton transporting membranes have been among the fundamental materials supporting a variety of modern electrochemical devices and sensors. The most frequently used one is Nafion®. The Nafion films have found many applications for proton transportation [1], energy storage [2], energy conversion [3], catalytic reaction media [4], and *in vivo* measurements of neurotransmitter [5]. The electrochemical characteristics the Nafion film and similar ionic polymer films as ion exchange polymer membranes were originally described in the pioneering publications [6-8].

A Nafion film immersed in water has a phase-separated structure composed of a micro water-phase and a perfluoroalkyl-phase. The water-phase is in a hydrophilic ionic channel as a micro water-domain surrounded by walls with condensed sulfonate groups of the side chains. The perfluoroalkyl-phase is a bulk region composed of perfluoroaklyl chains of Nafion. Because of the characteristic micro water-phase network structures, chemical micro-environment in a Nafion film has a specific electrostatic and hydrated nature. Studies on the basis of the two-phase framework model with the water-phase and perfluoroalkyl-phase were extensively conducted through various approaches from a viewpoint of micro-structures of hydrated Nafion films. Using the results of spectroscopic measurements of hydrated Nafion films by X-ray reflection and scattering and neutron-ray diffraction, a variety of nanoscopic and mesoscopic structure models have been proposed [9-15]. Inaba and co-workers pointed out the importance to consider the third phase enriched by the perfluoroether sites at the boundary of the aforementioned two phases [16]. Whichever two- or three-phase model is used, an understanding of chemical micro-environment of a Nafion film would provide us with an indispensable and practical guide to newly design a proton transporting membrane, because Nafion presently represents one of the best materials for polymer electrolyte fuel cells. We may also expect new applications of Nafion as a bi-continuous phase-separated material.

The spectroscopic methods frequently have difficulty in gaining a better insight into

the micro-phase structures in the hydrated Nafion films. On the other hand, analytical methods using molecule probes such as fluorescence probes [17-19], electron spin resonance probes [20], and redox probes [21-24] attain *in-situ* observation of chemical micro-environments in the hydrated Nafion films. Viologens as redox probes uncovered the ionic channel sizes in Nafion films from the diffusion and dimerization processes of the probes [23,24]. Mortimer and Dillingham found Nafion's permeation allowance for dihexyl viologen and forbiddance for diheptyl viologen [25]. This fact confirms the known diameter of the channel, being smaller than 4.2 nm [26]. The viologens exhibited superior molecular probe features, because they have reversible electrochemical activity. Both oxidized (V^{2+}) and one-electron reduced ($V^{\bullet+}$) forms are cationic species possessing affinity to the anionic sulfonate groups in the ionic channel of Nafion. Strongly colored nature of $V^{\bullet+}$-forms enables us to follow the state of viologen by visible spectroscopies. To our best knowledge, however, redox probes have been restricted so far to cationic and hydrophilic ones, which are perfluoro-repulsive. This has limited the obtainable properties of the micro-environments in Nafion. To shed light in more depth of the ionic channels, the use of a probe having a perfluoroalkyl affinity should be meaningful.

In this work, we use a perfluoroalkyl viologen redox probe, *N*,*N*'-di-(1*H*,1*H*,2*H*,2*H*-perfluorobutyl)-4,4'-bipyridinium dichloride (FC4VFC4), bearing perfluoroalkyl side chains. Electrochemical properties of FC4VFC4 have been reported elsewhere [27]. In the light of the above-mentioned diameter of the channel, the molecular size and water-solubility should allow for penetration of FC4VFC4 into Nafion films. FC4VFC4 in the Nafion film may have affinities to both perfluoroalkyl-phase and sulfonate groups simultaneously. We use a Nafion-coated polycrystalline Au electrode in the aqueous solution of FC4VFC4 and dibutyl viologen (C4VC4). C4VC4 is the alkyl analog of FC4VFC4 as a reference substance to highlight the effect of perfluorination of the side chains. Scheme 1 shows molecular structures of the two viologens. In addition to voltammetric measurements, electroreflectance (ER) spectral measurements are made to focus on the states and electron transfer reactions of viologen in a close proximity of the

Au electrode surface. We also track the penetration of viologen into the Nafion film by a combined use of CV and ER data.

Scheme 1.

2. Experimental

2.1. Material. Water was purified through a Milli-Q Plus Ultrapure water system coupled with an Elix-5 kit (Millipore Co.) to 18.2 MΩ cm. Materials used without further purification include Nafion 5 wt.% solution (Sigma Aldrich), KCl (Nacalai Tesque), and isopropanol (Sigma Aldrich).

2.2. Electrochemical and spectroelectrochemical measurements. All the measurements were conducted using a polycrystalline Au electrode with a surface area A = 0.0201 cm^2 with a PEEK sheath (BAS Inc.). Voltammetric studies were conducted using a Ag|AgCl|sat'd KCl or a Ag|AgCl|0.1 M KCl reference electrode and a coiled Au wire counter electrode. All the potentials in this paper are referenced to a Ag|AgCl|sat'd KCl. All the measurements were made under an Ar gas (> 99.998%) atmosphere at room temperature (25 ± 2°C). The electrochemical behavior of viologens was characterized at bare and Nafion-coated Au electrodes. The coating of the Au electrode surface with a Nafion film was conducted by casting 10 μL of 0.5 wt% Nafion/isopropanol solution homogeneously on both the centered circular Au of a diameter of 0.16 cm and surrounding PEEK coplanar ring-shaped surface (in total 0.283 cm^2). It was then dried in air. The thickness of the dry Nafion film on the Au surface was 1.0 ± 0.2 μm as measured by a scratching method of a contact mode AFM imaging. Before use, the Nafion film on the electrode was swelled by immersing the electrode in the supporting electrolyte solution free of viologen.

For the electrochemical measurements, a potentiostat (HECS 326, HUSOU) was employed. The base electrolyte solution in electrochemical measurements was 0.1 M KCl solution unless otherwise stated. For the time-course measurements of CVs, the time zero (t = 0 min) was set at the time when the Nafion-coated Au electrode was

immersed in a pre-deaerated viologen solution of a concentration of C_s in the electrochemical cell. At certain times, a single potential-cycle CV was recorded at a scan rate (v) of 200 mV s^{-1}.

The potential modulation used for the ER measurements is described as

$$E = E_{dc} + E_{ac} = E_{dc} + \Delta E_{ac}\text{Real}[\exp(j\omega t)] \quad (1)$$

where E_{dc} is the dc potential, E_{ac} is the ac potential, ΔE_{ac} is the zero-to-peak ac amplitude of the potential modulation, $j = \sqrt{-1}$, $\omega = 2\pi f$, where f is the modulation frequency, and t is the time. The instruments and procedures used for the ER measurements were described elsewhere [28]. Briefly, under the ac potential modulation, steady-state monochromatic light was irradiated to the electrode surface. The reflected light was detected by a photomultiplier (Hamamatsu R928) to analyze ac reflectance signal using a lock-in amplifier (EG&G, model 5210). The time-averaged dc reflectance, R_{dc}, was also monitored simultaneously. Normalization of the ac signal by R_{dc} gave the real part ER signal $(\Delta R/R)_{real}$ (in-phase component with respect to E_{ac}) and the imaginary part $(\Delta R/R)_{imag}$ (90° out-of-phase component). If the reflectance change follows E_{ac} without any retardation in phase, $(\Delta R/R)_{imag}$ should be zero.

The program for the combined ER and CV measurements was a train setting shown in Scheme 2. All the ER and CV were recorded until reaching saturation of CV. The scanned wavelength (λ) region was restricted to a narrow range, from 640 to 440 nm, to minimize condition change during the λ-scan. The E_{dc} for each ER spectral measurement was set at E_m read from the immediately preceding CV chart, where E_m is the midpoint potential of anodic and cathodic peaks of the viologen redox.

Scheme 2.

3. Results and Discussion

3.1. Voltammograms at a Nafion coated Au electrode.

The Nafion-coated Au electrode showed pronounced changes of CV with time. At given C_s, CVs at 200 mV s^{-1} were intermittently measured until reaching saturation. The total number of potential scans was restricted to prevent the CV from being influenced by the scans themselves. We monitored the redox reaction of $V^{\bullet+}/V^{2+}$ couple, $V^{2+} + e^-$ (electrode) $\rightleftharpoons$ $V^{\bullet+}$, and we did not scan the potential region of further reduction of $V^{\bullet+}$.

Fig. 1

3.1.1. C4VC4 at C_s = 500 μM. Fig. 1 shows the results of CV measurements in a 500 μM C4VC4 + 0.1 M KCl solution at a Nafion-coated Au electrode. Immediately after the immersion, a viologen redox peak pair appeared at E_m = -0.690 V (black line of t = 0 min in Fig. 1-a) together with a cathodic peak of residual oxygen reduction around -0.42 V. It is known that a bare Au electrode in 500 μM C4VC4 solution shows an electrochemically reversible CV response at E_m = -0.628 V [29]. A close look at the line of t = 0 min in Fig. 1-a ensures the absence of any trace of additional cathodic current ascribable to the reduction reaction of viologen between -0.63 V and -0.68 V; this is the proof for the Nafion-coated electrode prepared in this work that any macroscopic bare Au electrode area was not exposed to the solution. At t = 30 min, both the anodic peak current i_{pa} and the cathodic peak current i_{pc} reached maxima and then decreased slowly to be steady state values at t > 700 min. In a separate experiment, we stopped the time-course tracking at certain t and recorded sweep rate (v) dependence of CV (not shown here). The peak currents were proportional to the square root of v in the range of 10-200 mV s^{-1} regardless of t, indicating that diffusion of viologen largely determines the CV response.

Provided that the diffusion coefficient of the reduced form, D_{Red}, in Nafion is close to that of the oxidized form D_{Ox}, E_m can be approximated to the formal potential; it shifted from -0.690 V to less-negative to -0.595 V at 60 min, then shifted to slightly negative to reach a steady-state value, -0.620 V. The peak separation $\Delta E_p = E_{pa} - E_{pc}$ increased from

114 mV at 5 min to 372 mV at 360 min. The peak separations were larger than the ideal value for electrochemically reversible response of solution species (57 mV), indicating the sluggish electron transfer process at the electrode surface, the significant film resistance R_u, or non-negligible effect of migration because of the relatively low concentration of electrolyte cation. The quantitative analysis of the migration effect will be dealt with in our future work.

To examine the effect of R_u on CV, we measured electrolyte KCl concentration (C_{KCl}) dependence for 500 μM methyl viologen (MV) solution. The value of ΔE_p of the CV response of $MV^{\bullet+/2+}$ became greater with decreasing C_{KCl}; ΔE_p = 65 mV for C_{KCl} = 1.0 M, 101 mV for 0.1 M, and 226 mV for 0.01 M. The peak current at C_{KCl} = 1.0 M is about 1/5 of that with C_{KCl} = 0.1 M, indicating that partitions of MV^{2+} and K^+ from the solution phase into the Nafion film are competitive against each other. The higher C_{KCl} gives a lower MV concentration in the film and a higher ionic conductance through the ionic channel networks in the Nafion film, resulting in the decreases in both R_u and ΔE_p. The decrease of C_{KCl} elevated R_u and increased the saturated concentration of MV in the Nafion film. On the basis of the aforementioned results, the increase of ΔE_p with time can be attributed to the decrease of the electrolyte concentration in the Nafion film by the penetration of C4VC4. It is known that the ionic channel diameter depends on ionic composition in the channel [29]. Additional effect of narrowing of the ionic channel cross-section with time on the increase of ΔE_p is expected. In Fig. 1, we observed a rapid positive shift of E_m in the first 30 min. This would correspond to the increased fraction of $V^{\bullet+}$-dimers over its monomers in the reduction products. It is known that the formal potential of the dimer is more positive than that of a monomer [30].

Fig. 2

3.1.2. FC4VFC4 at C_s = 500 μM. Fig. 2 shows the results of the time course CV measurements in a 500 μM FC4VFC4 + 0.1 M KCl solution. The increase of the peak current in the first 10 min was followed by a steep decrease. After 30 min, the cathodic

peak ranged out of the negative end of the potential scan, *viz.* E_{pc} < -0.8 V. Finally, the CV reached a steady-state irreversible waveform after 720 min (Fig. 2-b). Fig. 2-c shows the time-dependent peak currents, and Fig. 2-d does the time-dependent peak potentials. Until 10 min after immersion, CVs exhibit distinct cathodic and anodic peaks, giving E_m around -585 mV. After the cathodic peak went out of the negative potential scan range, the anodic peak was still observable but gradually became smaller. FC4VFC4 displayed quite different behavior from C4VC4 at the same C_s (500 μM). The irreversible response of FC4VFC4 indicates its very sluggish electron transfer at the Au electrode surface and/or a very large R_u.

3.1.3. C4VC4: C_s dependence. Fig. 3-a shows the steady-state CVs for a Nafion-coated Au electrodes in C4VC4 solutions of three different C_s. The ΔE_p increased with the increase of C_s (184 mV at 5 μM, 254 mV at 50 μM, and 386 mV at 500 μM). Fig. 3-b shows the time dependence of i_{pc} after immersion in C4VC4 solutions. The absolute values of i_{pc} remained in the range of 4 - 8 μA, even though C_s differed by two orders of magnitude. This fact does not necessarily indicate that the amount of incorporated C4VC4 in the Nafion interior at C_s = 5 μM has already reached upper limit of the incorporation. The peak current should depend on several factors such as the surface concentration of V^{2+} in the proximity of the electrode surface, the diffusion coefficient, the active electrode area (the total surface area with which the water phase in ionic channels are in contact), the electron transfer rate constant k_s, and R_u. Although the surface concentration of viologen increases with time in the Nafion film, if the diffusion coefficient decreases and R_u increases because of the environmental change with the increased amount of viologen, the redox current cannot increase.

Fig. 3

3.1.4. FC4VFC4: C_s dependence. Fig. 4a shows steady-state CVs reached in the time-course measurements with three different C_s of FC4VFC4. Fig. 4-b shows the time

dependence of i_{pc}. Intriguingly, a better-defined redox response in CV was observed at a low concentration FC4VFC4 (5 μM) rather than at higher C_s. This concentration dependence is largely different from that of C4VC4 (Fig. 3). At 500 μM and 50 μM, a short time increase of i_{pc} was followed by sudden turndown to decrease (Fig. 4-b), resulting eventually in a significantly irreversible response. A similar trend was observed at 20 μM and 10 μM. The time period before the turndown is longer at lower C_s. To reach irreversible response after the current decrease, it took 1250 min at 20 μM and 4500 min at 10 μM. However, the redox current measured at 5 μM monotonically increased to reach a steady-state value, which was constant for over a few days at least. The CV at the steady-state was quasi-reversible, showing both cathodic and anodic redox current peaks with ΔE_p = 323 mV. We can conclude that there is a threshold concentration in between 5 and 10 μM to determine whether the critical damping of the CV of FC4VFC4 occurs or not.

To make the situation clear, it is desirable to estimate the concentration of FC4VFC4 in the film when C_s = 5 μM. It is known that, if a slow v limit of CV gives a thin-layer electrochemistry, the integrated charge of the CV peak should correspond directly the amount of active species [7,19,31]. Such a situation is realized when the partition at the film/solution interface is slow enough or diffusion in the film is much slower than the diffusion in the solution phase. Therefore, we measured the v-dependence of CV. The peak current was proportional to $v^{1/2}$ down to 1 mV/s, and the CV was still of reversible diffusion limited type with the peak-to-peak separation being 70 mV. The further decrease in v down to 0.1 mV/s altered the CV to a sigmoidal waveform attributable to the EC type reaction (electrocatalytic reaction) of residual oxygen plus apparent diffusion process of the viologen. Unfortunately, the present Nafion film/viologen systems for both C4VC4 and FC4VFC4 do not adopt to this classical method of estimation.

Fig. 4

3.2. ER studies at Nafion-coated Au electrode.

The conventional voltammetric techniques alone cannot shed direct and real-time light on the state of the viologen molecules reacting near the electrode surface. Among various *in situ* spectroscopic methods, UV-visible light reflection has advantages over others, because a viologen-incorporated Nafion film is transparent in the colorless oxidized state, and one-electron reduced viologen has strong absorption bands in the UV-Vis-near IR region. In the measured λ range in this work, V^{2+}-form is colorless, whereas $V^{\bullet+}$-monomer form has absorption bands at ca. 400 nm and 602-604 nm, and $V^{\bullet+}$-dimer form does at ca. 367 nm, 536 nm, and ca. 850 nm. The isosbestic point of monomer and dimer is at 552 nm. We can also distinguish $V^{\bullet+}$-monomer and dimer from the spectrum. The phase retardation of the ac reflectance signal from E_{ac} enables us to estimate k_s. Semi-quantitatively, the intensity ratio of real and imaginary part signals at a given λ, which is abbreviated as "r/i-ratio", is an indicator of the heterogeneous electron transfer rate; the greater the ratio, the greater the value of k_s [28]. Applying an ac potential modulation E_{ac}, we can selectively observe the viologen molecules undergoing the redox interconversion that gives the ac spectroscopic signal at the same frequency as E_{ac}. The phase retardation may originate from the slow electron transfer kinetics as well as the nonzero cell time constant determined by the double-layer capacitance, the film resistance, and bulk solution resistance. Taken together, the ER method, namely potential-modulated UV-vis reflectance spectroscopic method, provides us with highly valuable information of the interfacial reaction of viologen molecules. Unless the redox reaction involves the surface-deposited dense phase of colored electroactive species, an ER spectrum representing the redox reaction shows a difference absorption spectrum: the absorption spectrum of reduced form from which that of the oxidized form is subtracted [28,32].

Fig. 5

In Fig. 5, the initial ER spectrum at 4 min in C4VC4 solution shows no redox

response of viologen but a weak and broad ER signal from the Au surface as a negative-going real part response with a maximum around 500 nm [28] (also seen in Fig. 6-a). Growths of the ER signals of the redox reaction of viologens were obvious from 18 min in C4VC4 solution and from 19 min in FC4VFC4 solution. Because $V^{\bullet+}$-forms have strong visible absorptions but V^{2+}-form is colorless, the redox ER signals showed positive-going real parts and negative going imaginary parts. Because no surface deposition of $V^{\bullet+}$-forms took place, the spectral structure of the obtained redox ER signal was of the difference absorption spectral type.

In C4VC4 solution, the response of $V^{\bullet+}$-monomer at ~603 nm was first built up exclusively, and a rapid growth of the dimer signal at ~537 nm followed. The dimer signal became predominant over the monomer one after ca. 190 min. The same trend occurred in FC4VFC4 solution from much earlier time (30 min) than that in C4VC4 solution. These results confirmed that the ionic channel provides a volume for both C4VC4 and FC4VFC4 enough to find partner to form dimers. In addition, the concentration of $V^{\bullet+}$ became high enough to form its dimers by successive ingress of the viologens from the solution phase. In sharp contrast to the monotonical ER signal growth in C4VC4 solution for 500 min, the ER signal in FC4VFC4 solution decreased drastically after 163 min. After 4 h, the ER signal of FC4VFC4 redox almost disappeared.

Fig. 6

Fig. 6 shows typical ER spectra taken from Fig. 5. The zero-line is now added. Because the ER signal from the Au surface (Fig. 6-a) is relatively weak, provided that the cell time constant never affects the phase of redox ER signal, we can now discuss the r/i-ratio. In Fig. 6, with an increase in the ER signal of C4VC4, the r/i-ratio became smaller at both 537 nm and 603 nm. In contrast, ER spectra in FC4VFC4 solution exhibited a different r/i-ratio at 603 nm from that at 537 nm; for example, at t = 123 min the former was greater than the latter (Fig. 6-e). The ratio was also a function of t. We

can learn from Figs. 5 and 6: (i) The redox process of the monomer became sluggish with time for both C4VC4 and FC4VFC4, and (ii) The redox reaction of $V^{\bullet+}$-dimer/V^{2+} couple is relatively slower than that of $V^{\bullet+}$-monomer/V^{2+} couple. The following section is devoted to the discussion about the time-dependent features by combined use of CV and ER data.

3.3. Time-dependent behavior observed by CV and ER.

It is crucial to perceive the diffusion layer thickness of viologen in the Nafion film when measuring CV. Using a rotating-disk electrode (RDE) technique as follows, we confirmed that the diffusion layer thickness is thinner than the thickness of the hydrated Nafion film as far as $v > 1$ mV s^{-1} is used. First, RDE measurements in 0.5 mM MV solution were made for a hydrated Nafion film-coated Au-RDE. The film thickness was set as the same as that on the stationary Au electrode. We found that the CVs at $v > 1$ mV s^{-1} were never affected by the on-off of the rotation. In contrast at $v < 1$ mV s^{-1}, CV became smaller when stopping the rotation. The change of CV occurred when the tail end of the diffusion layer reached to the Nafion|solution interface. Second, recall that in the aqueous solution phase, the diffusion coefficients of C4VC4 and FC4VFC4 are 63.4% and 54.1% of that of MV in aqueous solution [23]. This fact gives a rationale behind the assumption that the diffusion coefficients of C4VC4 and FC4VFC4 in Nafion are also smaller than MV. Taken together, as far as a sweep rate of 200 mV s^{-1} is used, the tail of the diffusion layer is well inside of the Nafion film.

We should note the difference between a wide potential range CV and a smaller amplitude potential-modulated ER to gain comprehensive understanding of the spatiotemporal behavior. In CV measurements, the potential was scanned almost over the range of cathodic and anodic peaks, namely 0.0 to -1.0 V. When the CV current takes its peak, the diffusion layer is largely extended from the electrode surface to the interior of the Nafion film. On the other hands, in ER measurements, the electrode potential was repeatedly changed sinusoidally around E_{dc}, set at the formal potential, with a peak-to-peak amplitude of 113 mV (Eq. 1). The concentration profiles of the

diffusion layer are of undulated waves decaying from the electrode surface to the direction of the film interior. The thickness of the undulated concentration profile is much smaller in ER measurements than the extended diffusion layer in the CV measurements. The ER method can detect the change of the concentration ratio $V^{\bullet+}/V^{2+}$ at the close proximity of the Au surface. By the use of ER signals, the electron transfer kinetics is roughly represented by the r/i ratio. The magnitude of the redox ER signal is represented by

$$I_{ER} = [(\Delta R/R)_{real}^2 + (\Delta R/R)_{imag}^2]^{1/2} \quad (2)$$

where I_{ER} reflects the amount of viologens interconverted between oxidized and reduced states in response to E_{ac}; I_{ER} is greater when more viologens are reacted with faster kinetics [24].

Fig. 7

In Fig. 7, we can find the correlation among the CV cathodic peak current i_{pc}, CV peak separation ΔE_p, ER signal magnitude I_{ER}, and the r/i ratios. As far as the region of t < 350 min is concerned in 50 μM C4VC4 + 0.1 M KCl solution, the time dependence of I_{ER} was in line with i_{pc}. The increase of I_{ER} at 537 nm was steeper than that at 602 nm, indicating a steeper increase of the amount of $V^{\bullet+}$-dimer than the increase of $V^{\bullet+}$-monomer. In the region of t > 300 min, ΔE_p was almost constant, indicating that the electron transfer kinetics was unchanged and that iR drop caused by R_u was not substantial.

Taking a look at the time region of t < 300 min in 50 μM FC4VFC4 + 0.1 M KCl solution, we find sharply different time course behavior from that of C4VC4:

(i) Initially, the increases of I_{ER} and i_{pc} took place in parallel with keeping ΔE_p constant.

(ii) ΔE_p steeply increased after 163 min.

(iii) Before the increase of ΔE_p started, I_{ER} started decreasing at 97 min, while i_{pc} was still increasing

(iv) i_{pc} turned to decrease after I_{ER} reached to less than 30% of its maximum.

(v) When ΔE_p exceeded 400 mV, I_{ER} reached to less than 10% of its maximum.

(vi) When the ER signal further decreased to be almost zero, the cathodic peak went out of the scanned potential range.

The decrease in I_{ER} and the following increase in ΔE_p indicate that the interfacial electron transfer kinetics became sluggish or an increase in R_u occurred. We did not see any signature of the surface deposition of FC4VFC4 in the ER spectra. The r/i ratios of FC4VFC4 indicated that the monomer redox process is always faster than dimer reaction (Fig. 7-f), and for C4VC4 as well (Fig. 7-c).

If the decay of the redox response of FC4VFC4 is due to only the electron transfer kinetics, the increase of ΔE_p and the decreases of i_{pc} and r/i ratios should have occurred with the same time dependency. Because the observation is not in line, the time dependence originated from not only the slower kinetic but also slower diffusion and greater R_u but asynchronously. Therefore, a sudden change of the electron transfer kinetics alone is not likely.

Fig. 8

Fig. 8 shows dimer/monomer ratios calculated from Figs. 7-b and e applying Gao's method [33]. The values of I_{ER} at absorption maxima of monomer at 603 nm and dimer at 537 nm were used to calculate the ratio. The dimer/monomer ratio of C4VC4 was as low as 0.05 at the initial stage. Then, it increased to reach a constant value around 0.4 at 343 min, indicating that the concentration of the $V^{\bullet+}$-form of C4VC4 near the Au electrode surface attained saturation. In Fig. 1-d, it took much shorter time, 30 min, to reach saturation of the dimer content ratio in the solution of 500 μM C4VC4.

On the other hand, the dimer/monomer ratio for FC4VFC4 increased with time from t = 0 min to 163 min to be greater than 0.5. After ER signal of FC4VFC4 showed a rapid

decrease of the intensity, the dimer/monomer ratio value scattered. Note that the dimer/monomer ratios obtained from the ER spectra in 500 μM viologen aqueous solution on a bare Au electrode were 0.06 for C4VC4 and 0.22 for FC4VFC4. The enhanced dimerization in the Nafion film indicates the occurrence of concentration of these viologens in the ionic channels, and the extent of concentration became greater with time.

3.4. Additional messages delivered by the redox probe FC4VFC4.

The results of several additional key experiments using FC4VFC4 were listed herein.

(i) We examined whether the potential scan affected the results of the time course experiments. A newly prepared Nafion-coated Au electrode was dipped in 500 μM FC4VFC4 solution, kept it at the open circuit for 1 h, and then subjected to an initial potential scan. We obtained irreversible response almost the same as the intermittent experiments (Fig. 2). Because viologen is not reduced at the open circuit potential, this fact indicates that the potential scanning condition is not the prerequisite of the time course phenomenon and that the increase in R_u takes place even when only V^{2+} permeated the Nafion film.

(ii) We examined the redox reaction of ruthenium hexamine complex in the Nafion film. We observed a reversible, diffusion-controlled response of $[Ru(NH_3)_6]^{2+/3+}$ at a Nafion-coated Au electrode in the solution of 500 μM $[Ru(NH_3)_6]Cl_3$ in the absence of viologen. Because Nafion is a cation exchange membrane, abundantly incorporated $[Ru(NH_3)_6]^{2+/3+}$ underwent reversible redox reaction. When we changed the half of $[Ru(NH_3)_6]Cl_3$ to FC4VFC4 in the solution composition, the response of $[Ru(NH_3)_6]^{2+/3+}$ was largely diminished. The peak current of $[Ru(NH_3)_6]^{2+/3+}$ decreased to less than half, and ΔE_p became much greater, indicating a slower electron transfer rate of $[Ru(NH_3)_6]^{2+/3+}$. The final CV was of irreversible one. Note that no reduction of $[Ru(NH_3)_6]^{3+}$ mediated by viologen redox took place. When C4VC4 was used instead in the same experiment, apparent blocking of the redox of $[Ru(NH_3)_6]^{2+/3+}$ was not observed up to C_s of 500 μM.

(iii) We also examined CV response in the mixed viologen solutions, 250 μM MV + 250 μM FC4VFC4 and 250 μM C4VC4 + 250 μM FC4VFC4. In both solutions, the decay of the redox responses finally reached extremely irreversible ones as in Fig. 4-a. It is now clear that after the redox activity of FC4VFC4 is damped, even a coexistent smaller dialkylviologen cannot undergo quasi-reversible redox reaction.

(iv) We further examined the effect of relatively hydrophobic water-soluble cations including a perfluoalkylated one in the solution phase on the behavior of MV in a Nafion film. First, a Nafion film on a Au electrode was equilibrated in 500 μM MV + 0.10 M KCl solution to obtained a steady-state CV. Then, in the solution, butyl trimethylammonium ($(CH_3)_3N^+$-C_4H_{10}) chloride or *1H,1H,2H,2H*-perfluorobutyl trimethylammomium ($(CH_3)_3N^+$-C_2H_4-C_2F_5) chloride were added to make their concentrations be 2.0 mM. The peak current eventually decreased to 88% of initial value for the former, whereas it decreased to 80% for the latter. Importantly, more hydrophobic, perfluorinated tetraaklylammomium cation penetrated the Nafion through the ionic channels and more effectively displaced pre-incorporated MV.

3.5. Discussion on the experimental results and presumable models.

After the Nafion commenced to be used as a cation exchange and transport membrane of high performance following its invention in 1962, it has been long under debate how to understand the state and behavior of the cations in the ionic channels. The latest views can be found in literature. Wakai and co-workers discriminated three types of water in Nafion by using ^1H NMR, infrared, and mass spectroscopies, namely, condensed water, hydrated water, and strongly bound water on the sulfonate group [34]. Interconversion among these three states may take place. Shia and co-workers discussed the interaction of the sulfonate group sites on the inner wall of the ionic channel with incorporated cations [26] in terms of the change of water content. They claimed that, large and multivalent cations such as Cs^+ and Mg^{2+}, being different from small monovalent cations such as Li^+, Na^+, and K^+, tend to localize at the sulfonate site. If the

Nafion is not immersed in water but equilibrated in a low humidity atmosphere, the latter cations form cross-link structure together with sulfonate groups, because the localized interactive state behaves as an ion pair. But their discussion is limited to the case that electrostatic interaction is predominant.

Keeping these reports in mind, we describe a scenario of the time change of the state of viologens in the ionic channel in the Nafion film and the origin of the sharp contrast between perfluorinated viologen (FC4VFC4) and its alkyl analog (C4VC4). We have experimentally confirmed that both viologens can penetrate deep into the Nafion film to the electrode surface. It should be emphasized that the ionic channel of the Nafion can provide enough space for the $V^{\bullet+}$-forms to dimerize. In fact, the ER signal tracked both electroactive $V^{\bullet+}$-monomer and dimer species for both viologens (Figs. 5-8).

Because the total anionic charge of sulfonate groups in a Nafion film is constant, the increase of the incorporated amount of viologens leads to the decrease of K^+ concentration resulting in the increase of R_u. Regardless of the extent, this process takes place inevitably for both FC4VFC4 and C4VC4, and for MV as well. The viologen moiety is divalent (V^{2+}) or monovalent ($V^{\bullet+}$) cation being larger in size than the inorganic cations discussed in above mentioned work of Shia and coworkers [26]. Even when the Nafion film is hydrated in water, interaction between viologens and sulfonate groups should be significant.

The sharpest contrast between the two viologens is the fact that, although the redox response onsets and increases initially after immersion of the Nafion film in the solution, a turndown of redox activity of FC4VFC4 takes place. Not only the redox reaction of FC4VFC4 itself but also the reactions of smaller-in-size cationic species $[Ru(NH_3)_6]^{2+/3+}$ and MV were damped. This never happened for C4VC4 up to C_s = 500 μM. The redox activity is damped after CV curve becomes irreversible and ER signal disappears.

An important observation is given in (iv) of the section 3.4. Even the partly perfluorinated butyl trimethylammonium can penetrate in the ionic channel and displace pre-saturated MV in the Nafion film. This activity with partly perfluorinated butyl trimethylammonium was greater than that with the alkyl analog butyl

trimethylammonium, indicating the contribution of the attractive interaction of the perfluorinated butyl with the perfluroalkyl-phase of Nafion following the penetration through the ionic channel. This process is in line with the penetration of FC4VFC4, resulting in the damping of the response of coexistent MV.

In addition, a threshold solution concentration of FC4VFC4 is in between 5 and 10 μM. At lower concentrations of FC4VFC4 than 10 μM, the CV does not become irreversible. The structural difference between the two viologens is whether the end ethyl groups are perfluorinated or not. Therefore, the significant difference in the redox behavior should originate from either or both intermolecular and FC4VFC4-Nafion perfluoro chain-chain interactions. The interactions do not work on C4VC4. Three possible models to describe the scenario can be proposed.

Fig. 9

Model I. When the concentration of FC4VFC4 in the Nafion film is increased over a threshold, $V^{\bullet+}$ concentration as the reduction product reached its solubility limit in the ionic channels. We found in our previous work that FC4VFC4 has much lower aqueous solubility than C4VC4 because of intermolecular perfluoro chain-chain interaction [27]. This results in the precipitation in the film as C4VFC4-aggregates (Fig. 9) and a great extent of increase in R_u because of the narrowing of the ionic conductive pathways. Herein, predominant interaction is intermolecular perfluoro chain-chain interaction.

Model II. Both V^{2+}- and $V^{\bullet+}$-forms of $FC4V^{2+}FC4$ are strongly immobilized on the inside-wall of the ionic channel through not only electrostatic cation-sulfate interaction but also perfluoro chain-chain interaction with Nafion perfluoroether side chains (Fig. 9). Recall that the hydration state in the ionic channel is physically supported by mutual electrostatic repulsion between sulfonate groups on the inner wall of the channel. The neutralization of the negative charges on the inner wall by extensive accumulation of viologens at the wall reduces electrostatic repulsion between sulfonate groups, resulting in the loss of the driving force to keep the ionic channel in a well-swollen, expanded

state. Eventually, the ionic channels are narrowed and partially split, and R_u value becomes large.

Model III. Both intermolecular and FC4VFC4-Nafion perfluoro chain-chain interactions work synergistically. Aggregates of FC4VFC4 are produced because of the solubility limits. The aggregates undergo electrostatic and perfluoro chain-chain interaction with Nafion perfluoroether side chains (Fig. 9). Then, the ion channel is blocked.

Note that the Model I alone cannot explain the fact that, even when the electrode potential was kept at more positive potential of the formal potential of FC4VFC4, the CV became irreversible. To identify which model II or III is the most appropriate and to figure out which interaction is dominant or whether interactions are working synergistically or not, *in-situ* UV-visible and IR spectroelectrochemical measurements of the state of incorporated viologen are currently underway in our laboratory. The structure of ion channel in the presence of FC4VFC4 may be uncovered by using small angle X-ray Scattering and neutron reflection. Additionally, water uptake measurements *in an aqueous solution* should be needed.

In summary, FC4VFC4 gave us an unprecedented level of understanding of interaction of perfluoroalkyl cationic molecules with a Nafion film. Importantly, without the interactions brought about by the perfluoroalkyl chain, the electrostatic interaction alone does not induce apparent inhibition of the redox reaction.

4. Conclusions

Comparison of the redox behavior of FC4VFC4 and its alkyl analog C4VC4 was made in detail by a combined use of CV and ER. Because the difference between the two viologens was notable at the concentrations greater than 10 μM, our focus was on the range of higher concentrations. The results of the time course measurements after immersion of a freshly prepared Au/Nafion electrode into the viologen solutions of various concentrations gave us detailed information. Except for low concentrations (< 5

μM) of FC4VFC4, although the redox response onsets and initially increases, a turndown of redox activity of FC4VFC4 takes place. Not only the redox reaction of FC4VFC4 itself but also the reactions of $[Ru(NH_3)_6]^{2+/3+}$ and MV were damped. This never happened for C4VC4 up to C_s = 500 μM. The redox activity is damped after CV curve becomes irreversible and ER signal disappears. Without the interactions brought about by perfluoroalkyl chain, the electrostatic interaction alone does not induce apparent inhibition of the redox reaction. All the present experimental results and considerations allowed us to propose possible models in reference to recent reports. Those are Model II and III in Fig. 9, to describe the phenomena observed in this work. In conclusion, the new perfluorinated viologen probe provides us an unprecedented opportunity to shed deeper light into the interactions between organic cations and a Nafion film.

Acknowledgements

The authors acknowledge with appreciation to Dr. Hironobu Tahara at Nagasaki University for technical advices and useful discussions. This work was supported by a Grant-in-Aid (to TS) for Scientific Research on Innovative Area “Molecular Engine” (JSPS KAKENHI Grant Number JP19H05400) of The Ministry of Education, Culture, Sports, Science, and Technology, Japan. TA acknowledges to the Office of Research, Lakehead University and Dean of Graduate School of Engineering of Nagasaki University for enabling his short term stay for research work at the Department of Chemistry of Lakehead University.

References

[1] P. Choi, N.H. Jalani, R. Datta, Thermodynamics and Proton Transport in Nafion II.

Proton Diffusion Mechanisms and Conductivity, J. Electrochem. Soc., 152 (3) (2005) E123-E130.
https://doi.org/10.1149/1.1859814
[2] F. Lufrano, P. Staiti, Performance improvement of Nafion based solid state electrochemical supercapacitor, Electrochim. Acta, 49 (15) (2004) 2683-2689.
https://doi.org/10.1016/j.electacta.2004.02.021
[3] X.-L. Zheng, J.-P. Song, T. Ling, Z.P. Hu, P.-F. Yin, K. Davey, X.-W. Du, S-.Z. Qiao, Strongly Coupled Nafion on Molecules and Ordered Porous CdS Networks for Enhanced Visible-Light Photoelectrochemical Hydrogen Evolution, Adv. Mater., 28 (24) (2016) 4935-4942.
https://doi.org/10.1002/adma.201600437
[4] S.M. Jain, S. Tripathi, S. Tripathi, G. Spoto, T. Edvinsson, Acid-catalyzed Oligomerization via Activated Proton Transfer to Aromatic and Unsaturated Monomers in Nafion Membranes: A step forward in the in situ synthesis of Conjugated Composite Membranes, RSC Advances, 6 (2016) 104782-104792.
https://doi.org/10.1039/C6RA23105E
[5] M. W. Espenscheid, A. R. Ghatak-Roy, R. B. Moore, III, R. M. Penner, M. N. Szentirmay, C. R. Martin, Sensors from Polymer Modified Electrodes, J. Chem. Soc., Faraday Trans., 82 (1) (1986) 1051-1070.
https://doi.org/10.1039/F19868201051
[6] N. Oyama, T. Shimomura, K. Shigehara, F. C. Anson, Electrochemical Responses of Multiply-Charged Transition Metal Complexes Bound Electrostatically to Graphite Electrode Surfaces Coated with Polyelectrolytes, J. Electroanal. Chem., 112 (1980) 271-280.
https://doi.org/10.1016/S0022-0728(80)80409-8
[7] I. Rubinstein, A. J. Bard, Polymer Films on Electrodes. 4. Nafion-Coated Electrodes and Electrogenerated Chemiluminescence of Surface-Attached $Ru(bpy)_3^{2+}$, J. Am. Chem. Soc., 102 (1980) 6641-6642
https://doi.org/10.1021/ja00541a080

[8] P. Ugo, L. M. Moretto, Ion-Exchange Voltammetry at Polymer-Coated Electrodes: Principles and Analytical Prospects, Electroanalysis, 7 (12) (1995) 1105-1113.
https://doi.org/10.1002/elan.1140071202
[9] M. Fujimura, T. Hashimoto, H. Kawai, Small-Angle X-ray Scattering Study of Perfluorinated Ionomer Membranes. 1. Origin of Two Scattering Maxima, Macromolecules, 14 (5) (1981) 1309-1315.
https://doi.org/: 10.1021/ma50006a032
[10] W.Y. Hsu, T. Gierke, Ion transport and clustering in Nafion perfluorinated membranes, J. Membr. Sci., 13 (3) (1983) 307-326.
https://doi.org/10.1016/S0376-7388(00)81563-X
[11] G. Gebel, Structural evolution of water swollen perfluorosulfonated ionomers from dry membrane to solution, Polymer, 41 (15) (2000) 5829-5838.
https://doi.org/10.1016/S0032-3861(99)00770-3
[12] H.-G. Haubold, Th. Vad, H. Jungbluth, P. Hiller, Nano structure of NAFION: a SAXS study, Electrochim. Acta, 46 (10-11) (2001) 1559-1563.
https://doi.org/10.1016/S0013-4686(00)00753-2
[13] L. Rubatat , A.L. Rollet , G. Gebel , O. Diat, Evidence of Elongated Polymeric Aggregates in Nafion, Macromolecules, 35 (10) (2002) 4050-4055.
https://doi.org/10.1021/ma011578b
[14] K.S. Rohr, Q. Chen, Parallel cylindrical water nanochannels in Nafion fuel-cell membranes, Nat. Mater., 7 (2008) 85-83.
https://doi.org/10.1038/nmat2074
[15] K. D. Kreuer, G. Portale, A Critical Revision of the Nano-Morphology of Proton Conducting Ionomers and Polyelectrolytes for Fuel Cell Applications, Adv. Funct. Mater., 23 (43) (2013) 5390-5397.
https://doi.org/10.1002/adfm.201300376
[16] M. Inaba, J.T. Hinatsu, Z. Ogumi, Z. Takehara, Application of the Solid Polymer Electrolyte Method to Organic Electrochemistry: XV. Influence of the Multiphase Structure of Nafion on Electroreduction of Substituted Aromatic Nitro Compounds on Cu,Pt Nafion, J. Electrochem. Soc., 140 (3) (1993) 706-711.

https://doi.org/10.1149/1.2056146

[17] X.-Y. Yi, L.-Z. Wu, C.-H. Tung, Long-Lived Photoinduced Charge Separation in $Ru(Bpy)_3^{2+}$/Viologen System at Nafion Membrane-Solution Interface, J. Phys. Chem. B, 104 (40) (2000) 9468-9474.

https://doi.org/10.1021/jp001284c

[18] Y.P. Patil, T.A. P. Seery, M.T. Shaw, R.S. Parnas, In Situ Water Sensing in a Nafion Membrane by Fluorescence Spectroscopy, Ind. Eng. Chem. Res., 44 (16) (2005) 6141-6147.

https://doi.org/10.1021/ie0491286

[19] L.M. Moretto, T. Kohls, A. Chovin, N. Sojic, P. Ugo, Epifluorescence Imaging of Electrochemically Switchable Langmuir-Blodgett Films of Nafion, Langmuir, 24 (12) (2008) 6367-6374.

https://doi.org/10.1021/la703998e.

[20] T. Überrück, O. Neudert, K. Kreuerd, B. Blümich, J. Granwehr, S. Stapf, S. Han, Effect of nitroxide spin probes on transport properties in Nafion membranes, Phys. Chem. Chem. Phys., 41(20) (2018) 26660-26674.

https://doi.org/10.1039/C8CP04607G

[21] M. Shi, F.C. Anson, Some Consequences of the Significantly Different Mobilities of Hydrophilic and Hydrophobic Metal Complexes in Perfluorosulfonated Ionomer Coatings on Electrodes, Anal. Chem., 69 (14) (1997) 2653-2660.

https://doi.org/10.1021/ac970137g

[22] A. Yamauchi, Kazuki Togami, Ashraf M. Chaudryb, A. Mounir EL Sayed, Characterization of charged film of fluorocarbon polymer (Nafion) and blended fluorocarbon polymer (Nafion)/Collodion composite membranes by electrochemical methods in the presence of redox substances. V, J. Membrane Sci., 249 (1-2) (2005) 119-126.

https://doi.org/10.1016/j.memsci.2004.10.004

[23] A.M. Hodges, O. Johansen, J.W. Loder, A.W. H. Mau, J. Rabani, W. H. F. Sasse, Diffusion of viologens in Nafion film studied by a combined

electrochemical-spectrophotometric method, J. Phys. Chem., 95(15) (1991) 5966-5970. https://doi.org/10.1021/j100168a045

[24] O. Johansen, J. W. Loder, A. W. H. Mau, J. Rabani, W. H. F. Sasse, Properties of reduced viologens in Nafion films deposited on tin dioxide electrodes, Langmuir, 8 (10) (1992) 2577-2581.
https://doi.org/10.1021/la00046a036

[25] R. J. Mortimer, J. L. Dillingham, Electrochromic 1,1'-Dialkyl-4,4'-bipyridilium-Incorporated Nafion Electrodes, J. Electrochem. Soc., 144 (5) (1997) 1549-1553.
https://doi.org/10.1149/1.1837639

[26] S. Shia, A. Z. Webera, A. Kusoglu, Stracture-transport relationship of perfluorosulfonic-acid membranes in different cationic forms, Electrochim. Acta, 220 (1) (2016) 517-528.
https://doi.org /10.1016/j.electacta.2016.10.09

[27] T. Ayabe, B. Chan, T. Sagara, Fluorination effect of dibutyl viologen on its electrochemistry in aqueous solution, J. Electroanal. Chem., 856 (2020) 113691 1-6.
https://doi.org/10.1016/j.jelechem.2019.113691

[28] T. Sagara: In Advances in Electrochemical Science and Engineering, Vol. 9, Eds. C. Alkire, D. M. Kolb, J. Lipkowski, P. N. Ross, Wiley-VCH Verlag, Weinheim, pp. 47-95 (2006).

[29] P. N. Pintauro, R. Tandon, L. Chao, W. Xu, R. Evilia, Equilibrium Partitioning of Monovalent/Divalent Cation-Salt Mixtures in Nafion Cation-Exchange Membranes, J. Phys. Chem, 99 (34) (1995) 12915-12924.
https://doi.org/10.1021/j100034a034

[30] X. Tang, T.W. Schneider, J.W. Walker, D.A. Buttry, Dimerized π-Complexes in Self-Assembled Monolayers Containing Viologens: An Origin of Unusual Wave Shapes in the Voltammetry of Monolayers, Langmuir, 12 (24) (1996) 5921-5933.
https://doi.org/10.1021/la9503764

[31] P. Bertoncello, P. Ugo, Preparation and Voltammetric Characterization of Electrodes Coated with Langmuir-Schaefer Ultrathin Films of Nafion, J. Braz. Chem.

Soc., 4 (14) (2003) 517-522.
https://dx.doi.org/10.1590/S0103-50532003000400005
[32] T. Sagara, H. Murase, N. Nakashima, Frequency dependence of the electroreflectance signal for redox reaction of solution-phase species at the electrode surface: Formulation and experimental verification, J. Electroanal. Chem., 454 (1/2) (1998) 75-82.
https://doi.org/10.1016/S0022-0728(98)00232-0
[33] C. Gao, S. Silvi, X. Ma, H. Tian, A. Credi, M. Venturi, Chiral Supramolecular Switches Based on (*R*)-Binaphthalene–Bipyridinium Guests and Cucurbituril Hosts, Chem. Eur. J. 18(2012) 16911-16921
[34] C. Wakai, T. Shimoaka, T. Hasegawa, ^{1}H NMR Analysis of Water Freezing in Nanospace Involved in a Nafion Membrane, J. Phys. Chem. B, 119 (25) (2015) 8048-8053.
https://doi.org/10.1021/acs.jpcb.5b03568

Figure captions.

Scheme 1. Molecular structures of FC4VFC4 and C4VC4.

Scheme 2. Program used for combined ER and CV time-course measurements, showing the applied potential as a function of time. The time zero corresponds to the immersion of the Nafion-coated electrode in 50 μM viologen + 0.1 M KCl solution. For ER, ΔE_{ac} = 56.4 mV and f = 14 Hz.

Fig. 1. Time-course CVs for a Nafion-coated Au electrode (A = 0.201 cm^2) recorded in a 500 μM C4VC4 + 0.1 M KCl solution at v = 200 mV s^{-1} (a and subsequently b), and plots of peak currents (c) and peak potentials (d) *versus* time.

Fig. 2. Time-course CVs for a Nafion-coated Au electrode (A = 0.201 cm^2) recorded in 500 μM mM FC4VFC4 + 0.1 M KCl solution at v = 200 mV s^{-1} (a and subsequently b), and plots of peak currents (c) and peak potentials (d) *versus* time. The peak was distinctly observed until at the measurement of 240 min.

Fig. 3. Comparison of the steady-state CVs of a Nafion-coated Au electrode (A = 0.201 cm^2) at three concentrations of C4VC4 with the base electrolyte of 0.1 M KCl at v = 200 mV s^{-1} (a), and the time dependence of cathodic peak currents (b).

Fig. 4. Comparison of the steady-state CVs a Nafion-coated Au electrode (A = 0.201 cm^2) recorded at three concentrations of FC4VFC4 with the base electrolyte of 0.1 M KCl at v = 200 mV s^{-1} (a), and the time dependence of the values of their comparison of cathodic peak currents (b).

Fig. 5. Change of ER spectra with time after immersion of a Nafion-coated Au electrode in 50 μM C4VC4 + 0.1 M KCl solution (a) or 50 μM FC4VFC4 + 0.1 M KCl solution (b). E_{dc} for the potential modulation (see Eq. [1]) was set at the E_m in the latest

CV before the wavelength scan. Positive-going spectra (upper-going curves with red color) are of the real part, whereas negative-going spectra (lower-going curves with blue color) are of the imaginary part.

Fig. 6. Selected ER spectra obtained in 50 μM C4VC4 + 0.1 M KCl solution (a-c) and in 50 μM FC4VFC4 + 0.1 M KCl solution (d-f).

Fig. 7. Time dependence of the characteristic readout values from ER spectra and CVs in 50 μM C4VC4 + 0.1 M KCl solution (a, b, c) and 50 μM FC4VFC4 + 0.1 M KCl solution (d, e, f). (a) and (d): cathodic peak current i_{pc} and peak separation ΔE_p from CVs at 200 mV s^{-1}; (b) and (e), I_{ER} values (see Eq. 2) at three wavelengths, 603 nm as a monomer maximum in pale blue color triangles, 537 nm as a dimer maximum in gray squares, 552 nm as the isosbestic point in purple diamonds. (c) and (f) r/i ratios from ER spectra at the same three wavelengths as in (b) and (e).

Fig. 8. Time-course dimer/monomer ratios calculated from ER spectra recorded in 50 μM C4VC4 + 0.1 M KCl solution (closed circle), in 50 μM FC4VFC4 + 0.1 M KCl solution (closed diamond).

Fig. 9. Presumable models of the Nafion ion channel structure with saturated amount of FC4VFC4; **Model I**, FC4VFC4 aggregation model; **Model II,** Deposition on the inner wall surface model; **Model III,** Aggregation model including synergistically occurred deposition on the inner wall and FC4VFC4 aggregation.

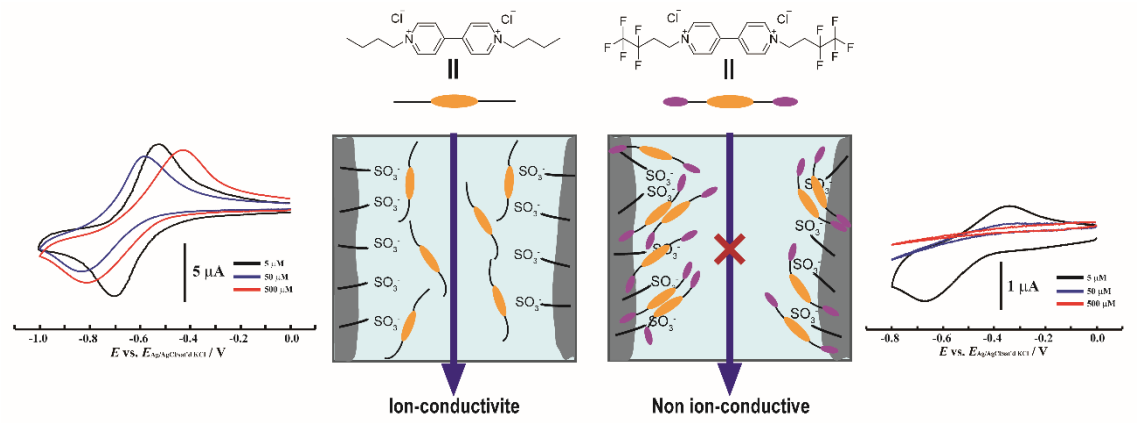

Graphical Abstract

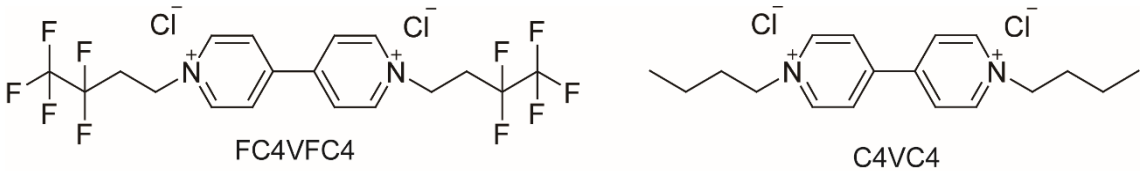

Scheme 1.

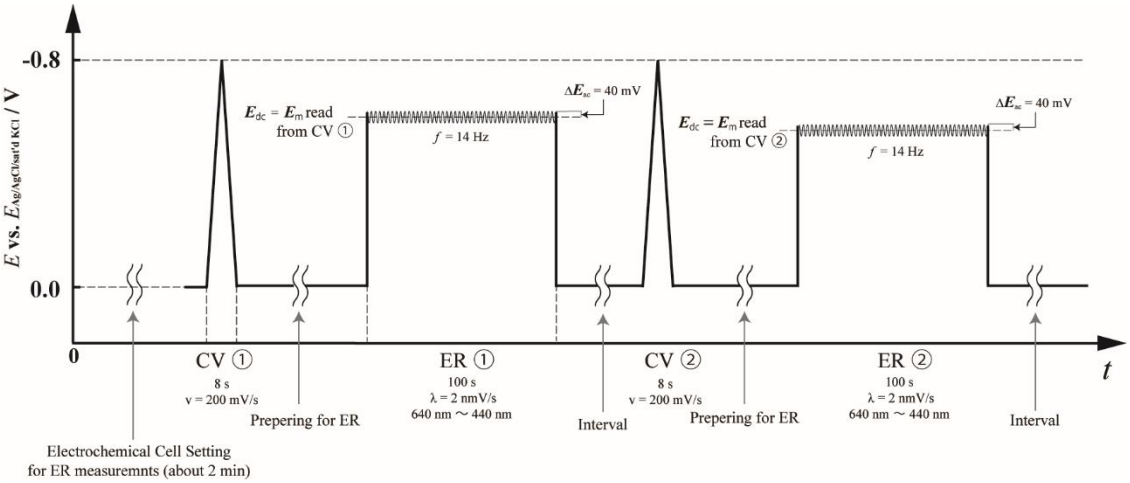

Scheme 2

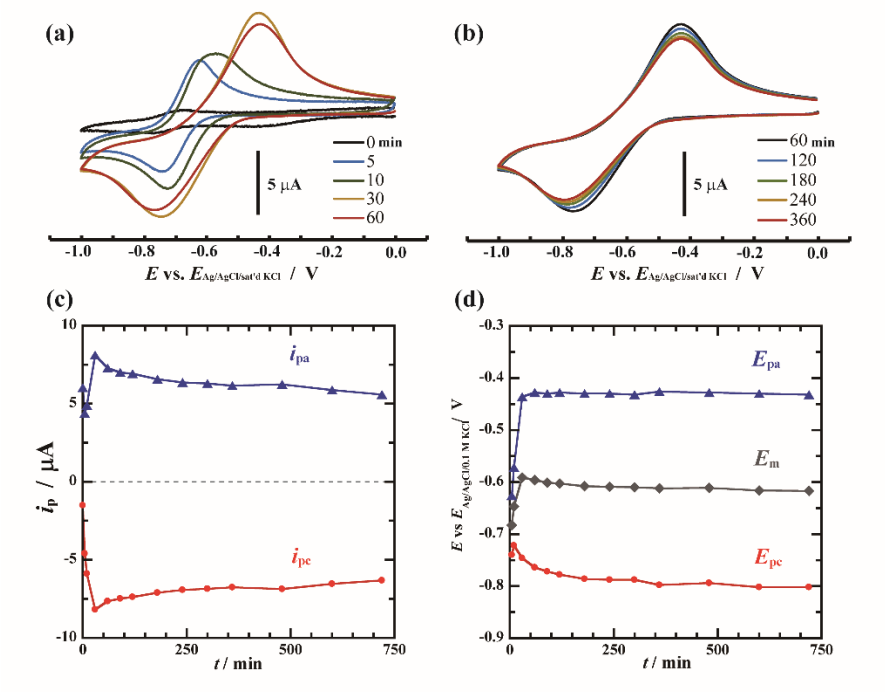

Figure 1

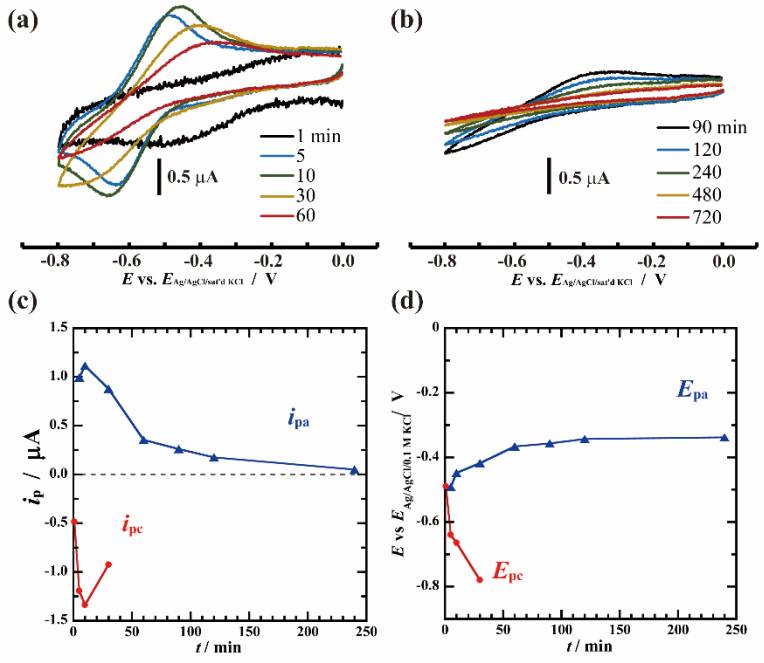

Figure 2

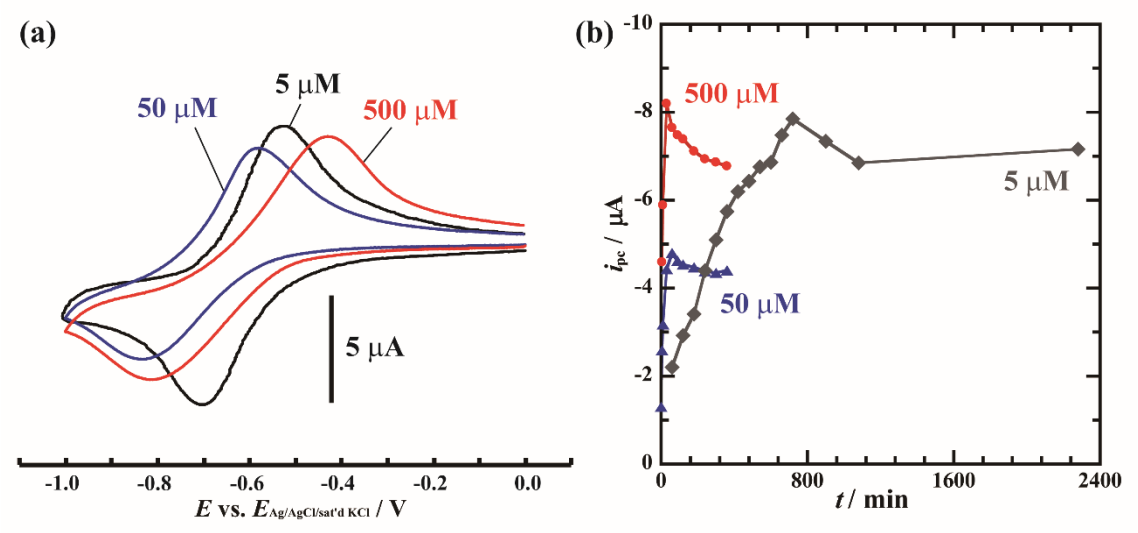

Figure 3

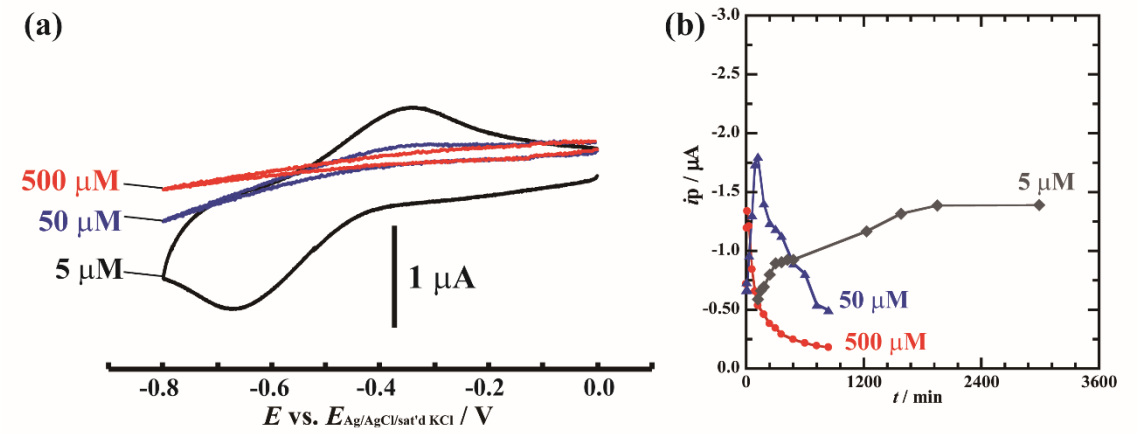

Figure 4

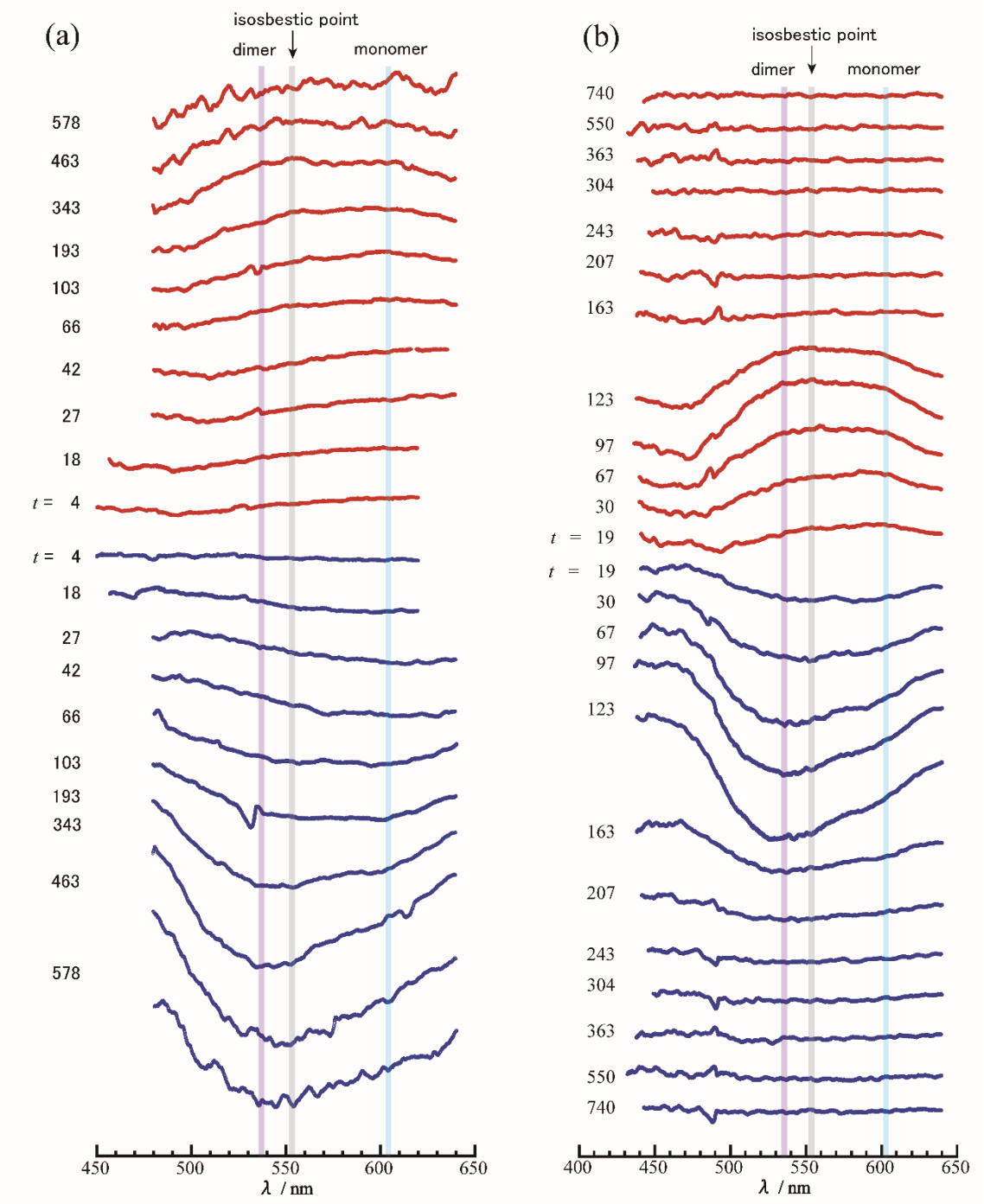
(a)
isosbestic point
dimer
monomer
578
463
343
193
103
66
42
27
18
t = 4
t = 4
18
27
42
66
103
193
343
463
578
450
500
550
600
650
λ / nm
(b)
isosbestic point
dimer
monomer
740
550
363
304
243
207
163
123
97
67
30
t = 19
t = 19
30
67
97
123
163
207
243
304
363
550
740
400
450
500
550
600
650
λ / nm

Figure 5

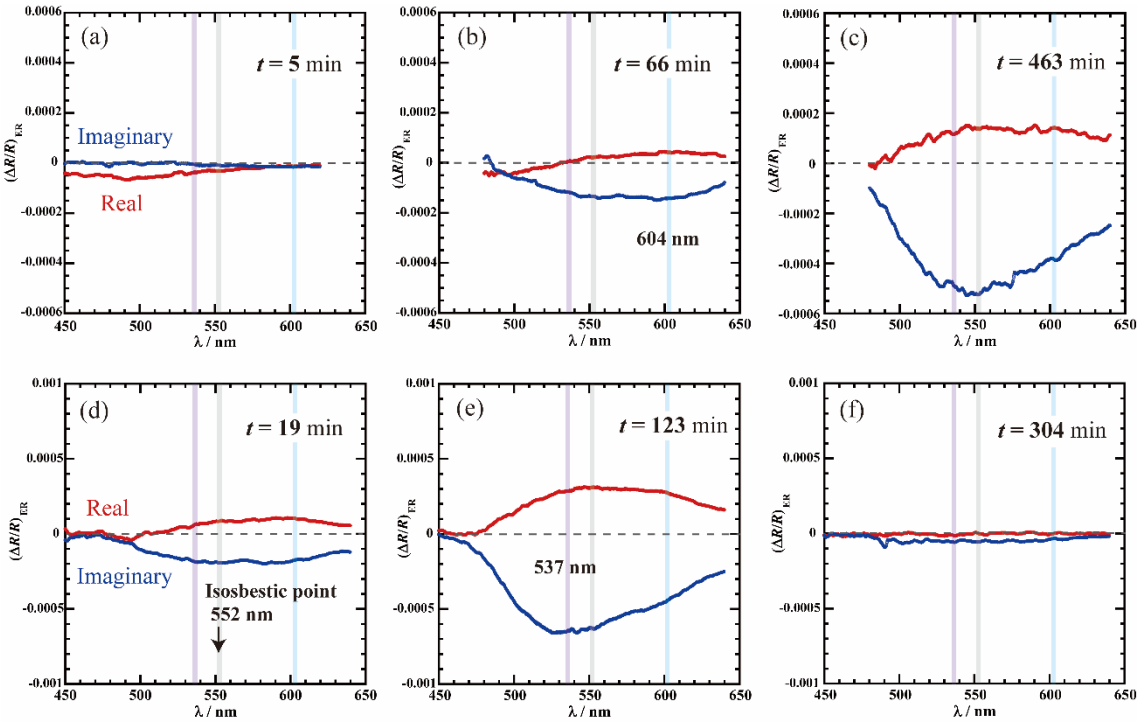
(a)
t = 5 min
Imaginary
Real
(b)
t = 66 min
604 nm
(c)
t = 463 min
(d)
t = 19 min
Real
Imaginary
Isosbestic point
552 nm
(e)
t = 123 min
537 nm
(f)
t = 304 min
λ / nm
(ΔR/R)ER
(ΔR/R)FR

Figure 6

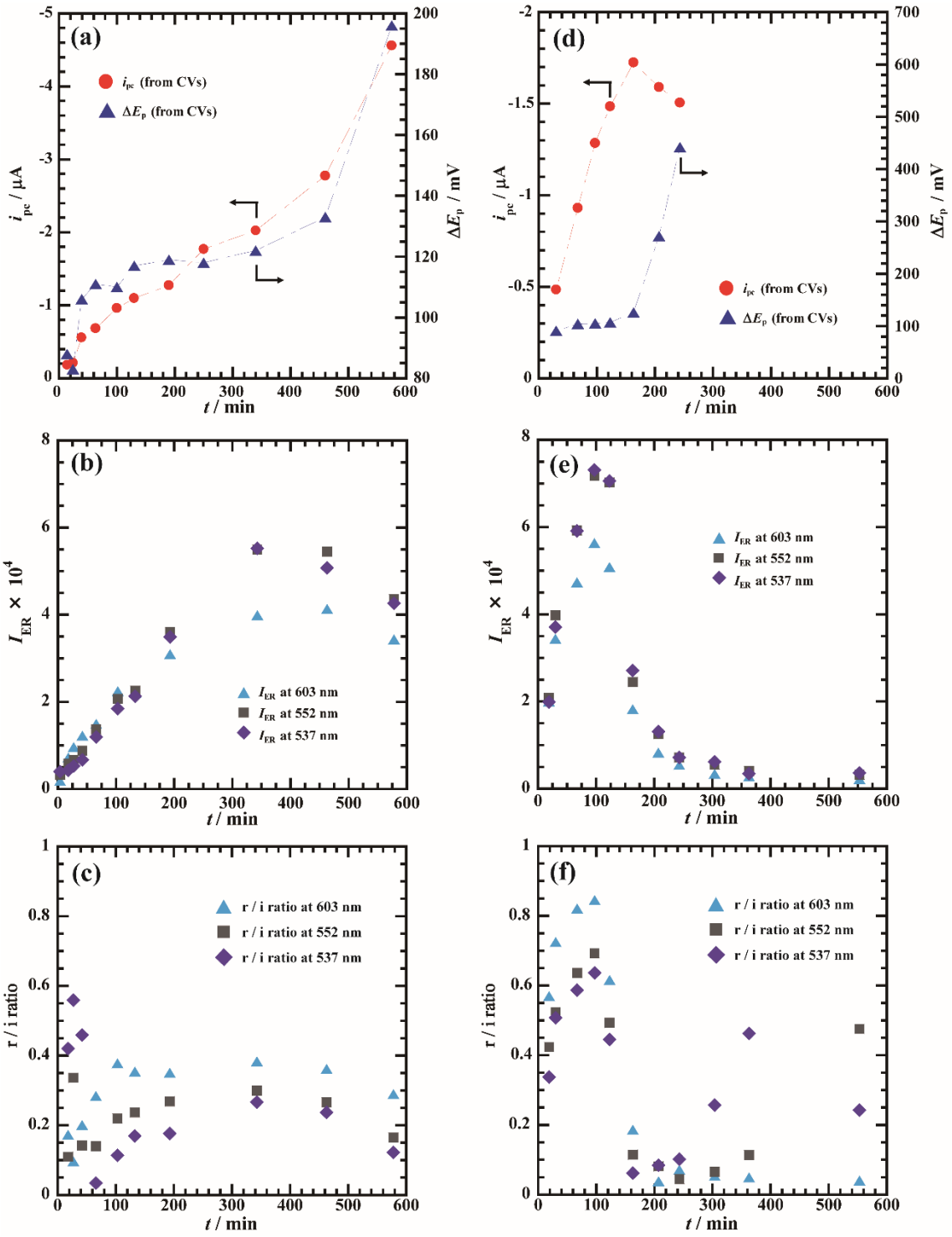
(a)
i_{pc} (from CVs)
ΔE_p (from CVs)
i_{pc} / μA
ΔE_p / mV
t / min
(d)
i_{pc} (from CVs)
ΔE_p (from CVs)
i_{pc} / μA
ΔE_p / mV
t / min
(b)
I_{ER} at 603 nm
I_{ER} at 552 nm
I_{ER} at 537 nm
I_{ER} × 10^4
t / min
(e)
I_{ER} at 603 nm
I_{ER} at 552 nm
I_{ER} at 537 nm
I_{ER} × 10^4
t / min
(c)
r / i ratio at 603 nm
r / i ratio at 552 nm
r / i ratio at 537 nm
r / i ratio
t / min
(f)
r / i ratio at 603 nm
r / i ratio at 552 nm
r / i ratio at 537 nm
r / i ratio
t / min

Figure 7

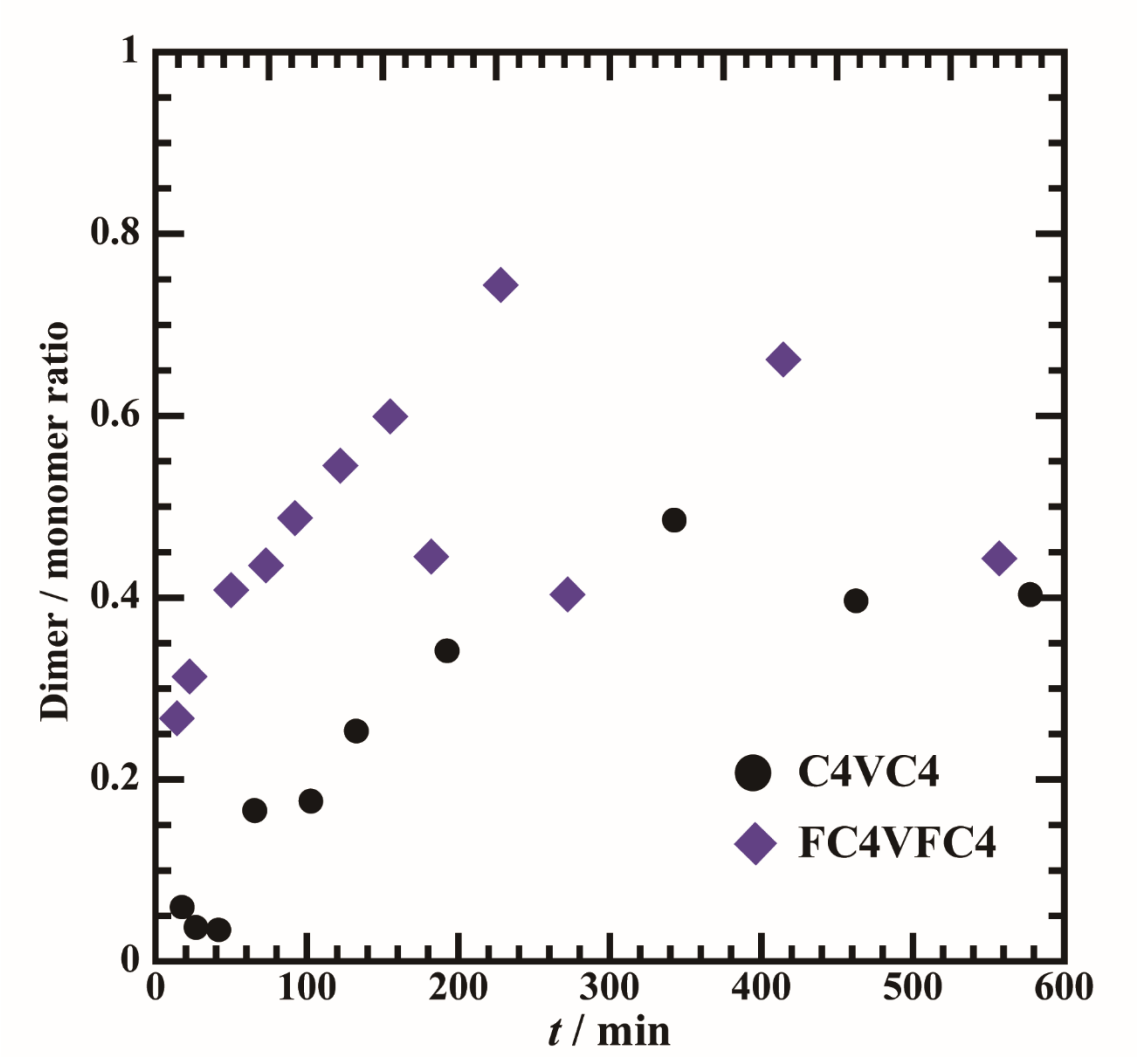
Dimer / monomer ratio
t / min
C4VC4
FC4VFC4
0
0.2
0.4
0.6
0.8
1
0
100
200
300
400
500
600

Figure 8

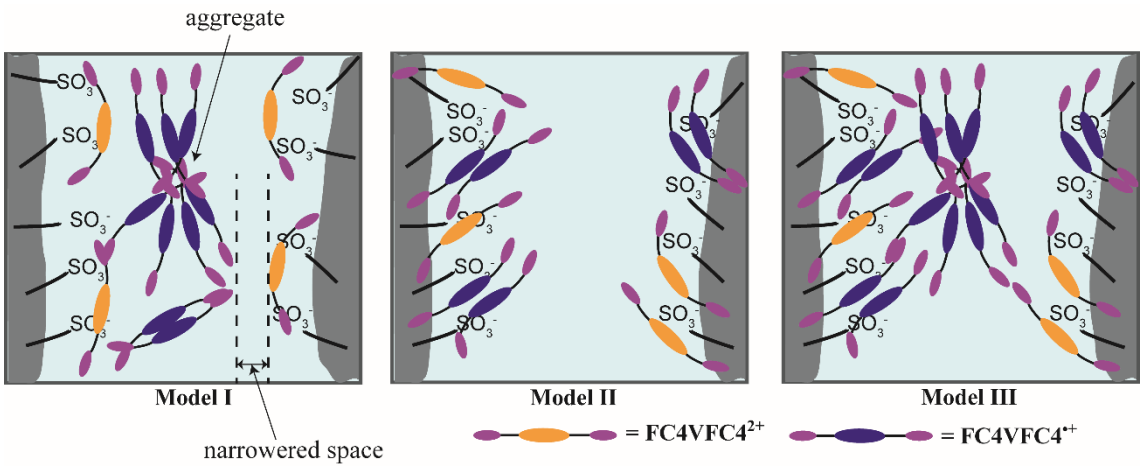
aggregate
Model I
narrowered space
Model II
Model III
= FC4VFC4^{2+}
= FC4VFC4$^{\bullet+}$

Figure 9